Giant enhancement of Raman scattering by a hollow-core microstructured optical fiber allows single exosome probing

Zhiwen Xia[a], Xin Zhang[b], Jingyuan Yao[b], Zihao Liu[a], Yulong Jin[b], Huabing Yin[c], Pu Wang[bde], and Xiu-Hong Wang[ade]*,

[a]Laboratory for Biomedical Photonics, and [b]Laboratory for Advanced Laser Technology and Applications, Institute of Laser Engineering, Faculty of Materials and Manufacturing, Beijing University of Technology; Beijing 100124 China

[c]Department of Biomedical Engineering, James Watt School of Engineering, University of Glasgow, Glasgow G12 8LT, the United Kingdom

[d]Key Laboratory of Trans-scale Laser Manufacturing Technology, Ministry of Education, Beijing 100124 China

[e] Beijing Engineering Research Center of Laser Technology; Beijing 100124 China

*Corresponding author:

Xiu-Hong Wang, Prof.

Beijing University of Technology, 100 Pingleyuan, Chaoyang District, Beijing 100124, China

Tel: 00-86-18612921803; Email: wxh2012@bjut.edu.cn

Key words:

Enhancement of Raman scattering, Hollow-core anti-resonant optical fiber, strong light-matter interaction, single exosome detection, cancer diagnosis.

Abstract

Microstructured optical fibers (MOFs) provide solutions for breaking through the bottlenecks in areas of high-power transmission and high-efficiency optical waveguide. Other than transporting light wave, MOFs can synergistically combine microfluidics and optics in a single fiber with unprecedented light path length not readily achievable by planar optofluidics configurations. Here we demonstrate that hollow-core anti-resonant optical fiber (HcARF) can significantly enhance Raman scattering by over three-orders-of-magnitude (EF≈5000) compared with a planar setup, due to the joint mechanisms of strong light-matter interaction in the fiber core and cumulative effect of the fiber. The giant enhancement enables us to develop the first optical fiber sensor to achieve single cancer exosome detection via a sandwich-structured strategy. This enables multiplexed analysis of surface proteins of exosome samples, potentially allowing an accurate identification of the cellular origin of exosomes for cancer diagnosis. Our findings could expand the applications of HcARF in many exciting areas beyond waveguide.

Microstructured optical fibers (MOFs), especially the most recent innovations of hollow-core anti-resonant optical fibers (HcARFs), provide solutions for breaking through the bottlenecks in areas of high-power transmission and high-efficiency optical waveguide [1]. The featured light-guiding properties of anti-resonant optical fiber (ARF) determines its unique advantages such as broadband transmission, strong light-matter interaction, low delay, low nonlinearity, low transmission loss and low dispersion [2], rendering them an ideal medium for communication, especially in the big data era.

Other than transporting light wave, HcARFs can synergistically combine microfluidics and optics in a single fiber with unprecedented light path length not readily achievable by planar optofluidics configurations. The combination of featured parameters allows ultrafast signal propagation through the fiber without significant distortions, opening a door to a vast range of biochemical applications. A recently reported low-nonlinearity hollow-core anti-resonant fiber can transmit a single pair of orthogonal polarization modes with cross-coupling on the scale of 10^{-10} m^{-1}; providing a leap in performance for photonics-enabled sensors and instruments [3]. As a fluid channel, HcARFs enables nL-μL level sample to be tested in gaseous or liquid form in the core, dispensing with a sample cell. Therefore, HcARFs have emerged as a powerful tool in the field of biochemical, gas, strain and temperature sensing [4-9], via taking advantages of the strong light-matter interaction. Light-gas-acoustic interaction and light-gas-thermal interaction in gas-filled HcARFs resulted in phase modulation of a probe beam propagating in the fiber, enabling spectroscopic characterization of gas species and concentration as well as the fiber microstructure [7-9]. Orders-of-magnitude enhancement of fluorescent signal by HcARF enabled ultrasensitive detection of environmental pollute [6, 10].

In view of enhancing Raman scattering using optical fiber, most reported studies

were focused on using hollow core photonic crystal fibers (HcPCFs). Previously, great successes have been achieved in enhancing Raman scattering via free-space propagation in order to achieve highly sensitive detection, for instance, surface enhanced Raman spectroscopy (SERS) [11], tip enhanced Raman spectroscopy (TERS) [12] and cavity enhanced Raman spectroscopy (CERS) [13], the most striking enhancement factor by several orders of magnitude has been reported. Compared with free-space propagation, there are advantages using optical fiber to enhance Raman signal. For example, optical fiber is gifted with striking cumulative effect due to extended length. For the most of the cases, the volume of light-sample interaction of free-space propagation, which is proportional to Raman signal intensity, is extremely small. Tiny impurities would severely interfere with the assays, hindering the applications of the existing mechanisms. Considering the complexity of biological and clinical samples, low content of the target, as well as the necessity of point-of-care monitoring, additional technologies favoring for clinical applications is in urgent demand. In this regard, marriage of optical fiber approach with SERS/TERS/CERS may provide a solution.

Using hollow core photonic crystal fiber (HcPCF), highly sensitive detections of cancer marker epidermal growth factor receptors (EGFRs), heparin, leukemia cells, and so forth, have been reported [14-19]. However, HcPCFs suffer from numerous drawbacks that limit their use for SERS based biosensing and other opto-fluidic applications [20], which include: (a) transmission window is rather narrow, (b) the properties could be deteriorated by light coupling to modes confined in the ring of glass surrounding the hollow core [21] and (c) the evanescent field and the cladding mode of HcPCF often generate strong background Raman signal of silica material, interfering with the measurements. To block the background signal, additional device, such as a spatial filtering system with a small pinhole, need to be adopted [15]. These weaknesses severely

hamper the applications of Raman-based HcPCF sensor, especially for real-time monitoring of clinical samples. Other types of optical fibers, such as metal-lined hollow core fiber (MLHCF), suspended core optical fiber (SCF), have also been investigated for sensing applications, however, the transmission loss is rather high and, sometimes, are not appropriate for specific and label free detection [22-24].

The advantages of state-of-the-art HcARFs have attracted increasing attention in the sensing area. It is in this context; we investigated the Raman enhancing effects of HcARF and subsequently developed a novel HcARF-based surface enhanced Raman scattering (SERS) sensing platform for label-free and ultrasensitive detection of cancer exosomes in an extremely low sample volume. As proof of concept, cancer derived exosomes were analyzed quantitatively. Highly specific single exosome probing was achieved, moreover, surface protein profiling and multiplexed exosome identification to allow assignment of cancer subtypes were explored.

Experimental section

Fabrication and characterization of the HcARF

Silica tubes were pre-drawn into capillaries, and then stacked in silica outer sleeve to form an optical fiber preform. The fiber preform was placed in the high-temperature drawing tower and was drawn to form the designated microstructure.

The cross-section morphology of the as-fabricated optical fiber was analyzed using scanning electronic microscope (SEM, SU9000 STEM/SEM, Hitachi High-Technologies Corporation of Japan).

The transmission band was measured using a supercontinuum light source. Briefly, the laser of the supercontinuum light source was coupled into the 10cm HcARF (or

LcARF). The spot at the output end was recorded with a CCD, and the transmission spectrum was recorded by a spectrometer.

Numerical simulation

The light field distribution of HcARF and LcARF and the transmission losses were simulated using COMSOL Multiphysics. Only confinement loss was analyzed. The effective refractive indices of HcARF and LcARF at different wavelengths of optical transmission were utilized. According to the confinement loss formula, the loss value in the 0.4-1.5μm band was simulated.

Raman scattering signal measurement

For the planar substrate experiment, 10 μL Ag-4-MBN solutions at different 4-MBN concentrations were dropped on glass slides followed by immediate acquisition of Raman signal as described below. For optical fiber and capillary experiments, same length (10 cm) of capillary (50 μm diameter, TSU050375, Polymicro technologies) and HcARF fiber were filled with different concentrations of Ag-4-MBN solution via an autosampler. Raman spectra were acquired using a confocal Raman spectrometer (Renishaw inVia) with a 50× objective. A 785 nm laser was used to excite the samples. Data acquisition conditions were kept same for all the samples (excitation power 0.6 mW, acquisition time 10 s). The beam size of the excitation light was about 1μm. The signal obtained was from the total excitation zone.

The Raman enhancement factor (EF) was calculated using the following Eqn.1 [25]:

$$EF = \frac{\frac{I_F}{C_F}}{\frac{I_N}{C_N}} \quad (1)$$

Where I_F represents the intensity of the Raman signal in LcARF and I_N represents the intensity of the Raman signal on the planar substrate. C_F and C_N are the

concentrations of the 4-MBN molecule.

Fiber Surface Functionalization

The mixture of APTES, absolute ethanol and ultrapure water at concentration of 2.5%, 96.5% and 1% (v/v) was injected into the fiber channel using a precision injector (Baoding Leifu Fluid Technology Co., Ltd, China). After standing at room temperature for 6 h, the fiber was washed with water. The carboxylated AptCD63 was first activated by EDC and NHS solution (EDC and NHS were mixed at 1:1 ratio, then added to to 40 μL pH=5.85 MES buffer containing AptCD63) before filled into the fiber channel. After overnight incubation at room temperature, BSA (1 mg/mL) was filled to the fiber channel to shield the electrostatically active sites on the inner wall of the fiber. AptCD63-Cy5 was immobilized on the fiber wall using similar protocol. The above-mentioned functionalized fiber was washed with water, and then placed in the optical path in Fig. S3 for fluorescence measurement.

Construction of SERS probes

To prepare SERS probe for HER2, 4 μL 5 μM AptH2 was added to 100 μL 0.03 nM AgNPs solution, and incubated at 37°C for 2 h. Then, 8 μL 0.7 mM 4-MBN was added and incubated at room temperature for 3 h. The resultant SERS probes were purified by centrifugation (Thermo scientific) at 8000 rpm for 30 min, followed by removal of the supernatant. The probes were then dispersed in PBS. 5 μL of SERS probes was dried on silicon wafer for Raman spectrum measurement with a confocal Raman spectrometer. The zeta potential of SERS probes was measured using a Mastersizer 3000 (Malvern Panalytical).

Exosome detection using the proposed sensor

The SkBr3 exosomes were filled into the functionalized ARF using a precision liquid filling instrument at a speed of 1 μL/min and then incubated at 37°C for 2h. Then

SERS probe for HER2 was streamed in the fiber and incubated overnight at room temperature to allow the HER2 probe to specifically bind to SKBR3 exosomes. After thoroughly washed with ultrapure water, the fiber was placed on the operating platform for Raman spectra acquisition. A confocal Raman spectrometer (Renishaw inVia) with a 50× objective was used to detect SERS spectra. The SERS spectra were acquired at 785 nm excitation (the power was 0.6mW), the integration time was 10s.

Statistical analysis

Each experiment was repeated at least three times. The data was processed by OriginPro 2019b software and expressed as mean ± SD. One-way ANOVA was performed to judge whether the data are statistically significant, *** indicates that p value is less than 0.001, ** indicates that p is less than 0.01, and * indicates that p is less than 0.05.

Results and discussions

Fabrication and characterization of HcARF

The light guiding mechanism of anti-resonant fiber (ARF) follows the principle of anti-resonant reflecting optical waveguide (ARROW), as shown in Eqn. 2., where n is the refractive index of the fiber material, i.e. silica (n=1.45), n_l is the refractive index of the core, t is the wall thickness of the seven cladding holes, m=0, 1, 2…. HcARFs allow the match of low refractive-index (RI) fluids, resulting in a strong light-sample overlap in the core.

$$\lambda_{\mathrm{res}} = \frac{2\mathrm{t}}{\mathrm{m}}\sqrt{\mathrm{n}^2 - n_l^2} \qquad (2)$$

The resonance condition is usually determined by the thickness of cladding tube wall and silica refractive index. The core size and cladding tube size of HcARF were premeditated according to the required transmission wavelength and single-mode

transmission characteristics. Then, the HcARF fiber was fabricated using the Stack-and-Draw method [26]. Briefly, the capillary tubes were stacked inside to form a preform and drawn uniformly at high temperature. The cross section of as-fabricated HcARF was shown in Fig.1a. The outer diameter was 202 μm, the air core diameter D was 30 μm, the cladding tube diameter was 14 μm, and the wall thickness t of the cladding tube was 0.4 μm.

The transmission spectrum was shown in Fig. 1b (purple line). The anti-resonant transmission windows of a 10cm HcARF, measured using a supercontinuum light source (400-1200nm), were 470-750nm and >830nm (>1000nm was not measured). Since the fiber was attempted for sensing aqueous samples, the transmission spectrum of a liquid-core ARF (LcARF) was measured using the same supercontinuum light source, as shown in Fig. 1b (orange line). Mainly single-mode guidance was observed for both HcARF and LcARF, Fig. 1b inset. Excellent light transmission in the range of 470~1000 nm was observed for LcARF, which is in contrast to HcARF. The better light transmission in the range of 750-830nm of LcARF can be explained using Eqn. 2, which evidences that the transmission window of ARF is related to the refractive index contrast between cladding glass and core material. The resonant wavelength λ_{res} decreases, when the core material is changed from air (n=1) to water (n=1.33), which is spectrally manifested as a blue shift of the resonant band [27]. As a result, the resonant band (non-light conductive band) for HcARF at 750-830nm converted to light conductive band for LcARF, which is a benefit for using 785nm laser to excite Raman signal. Please note that, due to the wavelength limitation of the spectrometer, we were unable to observe blue shift of transmission band at the short wavelength region (around 400nm).

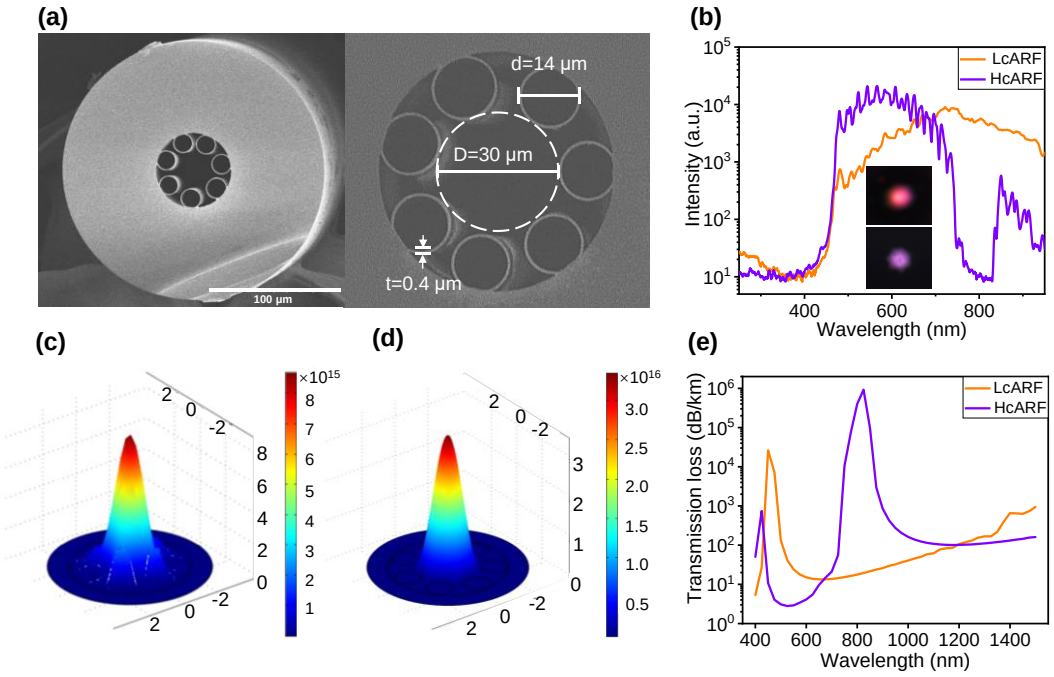

Fig. 1. Characterization of the HcARF and LcARF. **(a)**. Left panel: cross section morphology of the HcARF; right panel: microstructure of the cladding and the core. **(b)**. Transmission window of HcARF (purple line) and LcRF (orange line). The insets show mainly single-mode profiles of HcARF and LcARF respectively. **(c)**. Light electric field distribution in the core region of HcARF (left) and **(d)** LcARF (right). **(e)**. Simulated transmission loss of HcARF (purple line) and LcARF (orange line).

A striking feature of hollow-core anti-resonant optical fiber is the strict light confinement in the fiber core, due to the unusual light transmission mechanisms [28]. In addition, the specially-designed microstructure also enables light to be propagated at very low transmission loss [29, 30], in clear contrast to free space transmission. The overall effects ensure strong light-matter interaction in the core region.

To confirm that, the light electric field distribution of the fundamental guiding mode of HcARF and LcARF were simulated using finite element analysis method, as shown in Fig. 1c. At 785 nm, the light field distribution of LcARF (Fig. 1d) showed maximum intensity at the core center, ensuring strong light-matter interaction within the liquid core. These results provide strong evidence that the liquid core is a robust

waveguide, although the refractive index of the filled liquid (n=1.33) is much higher than air (n=1.0).

The simulated transmission losses of HcARF and LcARF were shown in Fig. 1e (here we only simulated the confinement loss). A resonant peak with maximum wavelength of ~800 nm for HcARF was observed (purple line), which is consistent with the transmission band (Fig. 1b purple line). For LcARF, the resonant band was present at around 430nm. This is consistent with the measured transmission spectrum in Fig. 1b orange line. Clearly, this property of LcARF favors Raman signal acquisition using 785nm excitation wavelength.

ARF enhances Raman scattering (AERS)

To investigate the fiber enhanced Raman scattering, the HcARF was filled with a mixture of AgNPs and 4-Mercaptobenzonitrile (4-MBN) solution and excited with a 785nm laser (Fig. S1). Fig. 2a, b & c are the Raman spectra of 4-MBN from a planar substrate (glass slide), a capillary tube, and a HcARF, respectively. A prominent peak of Raman shift at ~2223 cm^{-1} was observed owing to the stretch of C≡N triple bond, while the other two prominent peaks of Raman shift at 1585 and 1074 cm^{-1} were assigned to the symmetric in-plane aromatic ring C–C deformation and the C–H deformation, respectively [31]. Analyzing the data in Fig. 2a, b & c, great Raman signal enhancement was obtained. The Raman enhancing factors (EF) were over three-orders-of-magnitude, which were 2.43×10^3 and 4.89×10^3, when compared LcARF with capillary tube; and LcARF with planar substrate, respectively, which is the best record for optical fiber enhanced Raman scattering.

The remarkable enhancement of Raman scattering by ARF can be explicated by the joint effects of strong light-confining ability of ARF and the cumulative effect of

the fiber. The former enables maximum light-matter overlap within the liquid core, thus effectively amplifies the Raman scattering signal. Consistent with this, as a negative control, the capillary tube (with same length and similar diameter), which was unable to confine light within the liquid core due to absence of the microstructured geometry, failed to efficiently enhance the Raman signal. The cumulative effect arose from the fact that ARF fiber elongated the laser beam waist owing to the light confinement effect, therefore, allowing the laser beam waist to interact with extended sample length (Fig. 2d) than that of the planar substrate where the spot was limited by the scattering volume at the spot's focal point. The Raman scattering signal intensity (P) can be expressed by Eqn. 3[32, 33].

$$P \propto \sum_{i=1}^{M} \sigma_i I_i = M\sigma I_0 = m\sigma V I_0 \quad (3)$$

Where σ is the Raman scattering cross section of a molecule, I_0 is the average light intensity of pumping laser at the location, V is the excited sample volume, m is the molecular density. Clearly, increasing the light intensity is an effective way for enhancing Raman signal, as in the cases of SERS, TERS and CERS, in which enhancements are originated from the localized field enhancement based on the near field effect of metal nanostructure or circulated light in the cavity. In the case of fiber enhanced Raman signal, increasing the excitable sample volume plays a major role in signal enhancement, which may be impractical for free-space propagation, while can be easily realized using ARF. More importantly, the ARF fiber not only provide a means to increase sample volume, also, the fiber is gifted with light-converging ability due to the strict light confinement via the special micro-geometry, as shown in Fig.2d, ensuring strong light-matter interaction, and thus enabling efficiently enhancement of

Raman signal, which is a striking advantage compared with free-space propagation.

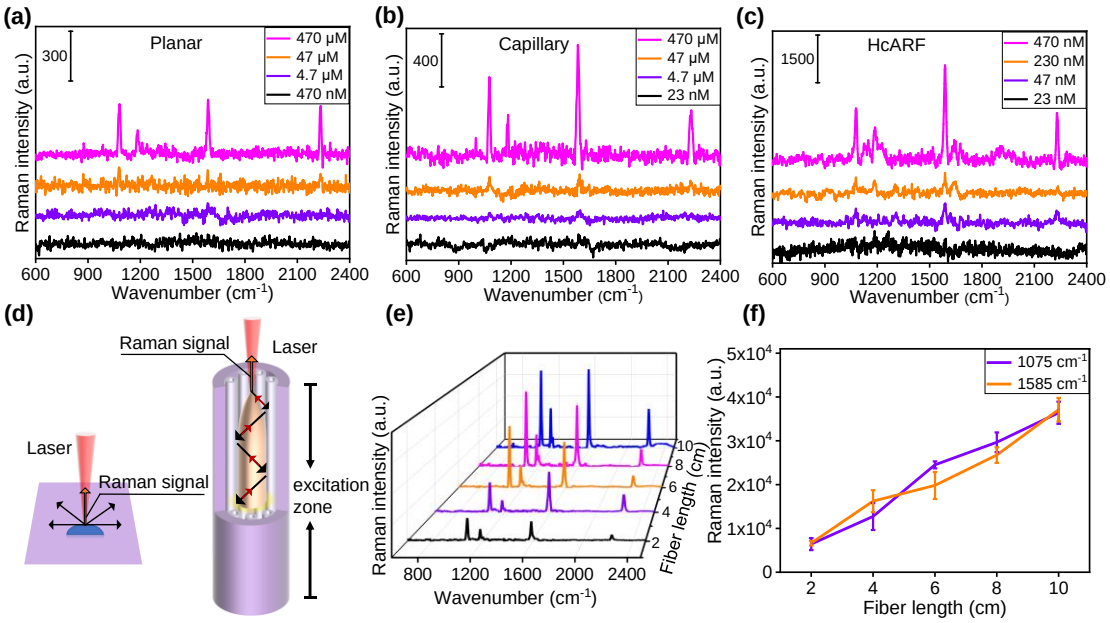

Fig. 2. HcARF enhances Raman scattering signal. **(a), (b) & (C)**. Raman spectra of 4-MBN obtained on a planar substrate (a), capillary tube (10cm in length, 50μm diameter) (b) and HcARF (10cm) (c), respectively. **(d)**. Schematic diagram showing the enhancing mechanism by HcARF. **(e)**. Raman spectra obtained using various lengths of HcARF. **(f)**. Length-dependent Raman signal at wavenumber of 1075 cm^{-1} (purple) and 1585cm^{-1} (orange). Ex. 785nm, laser power 0.6mW.

The cumulative effect could be demonstrated by the signal enhancement brought by increase of fiber length. We explored the effect of fiber length on Raman intensities by back-cutting the fiber, and the results were shown in Fig. 2e & f. Raman signal was positively correlated with the fiber length, providing a way to further intensify the signal. Considering the attenuation caused by sample absorption and particle scattering, etc, a maximum intensity would be reached at certain fiber length. Due to limitation of the setup (the maximum working distance is 10cm), we were unable to further investigate the effect of fiber length.

ARF sensor for exosome detection

Working principle of the sensor

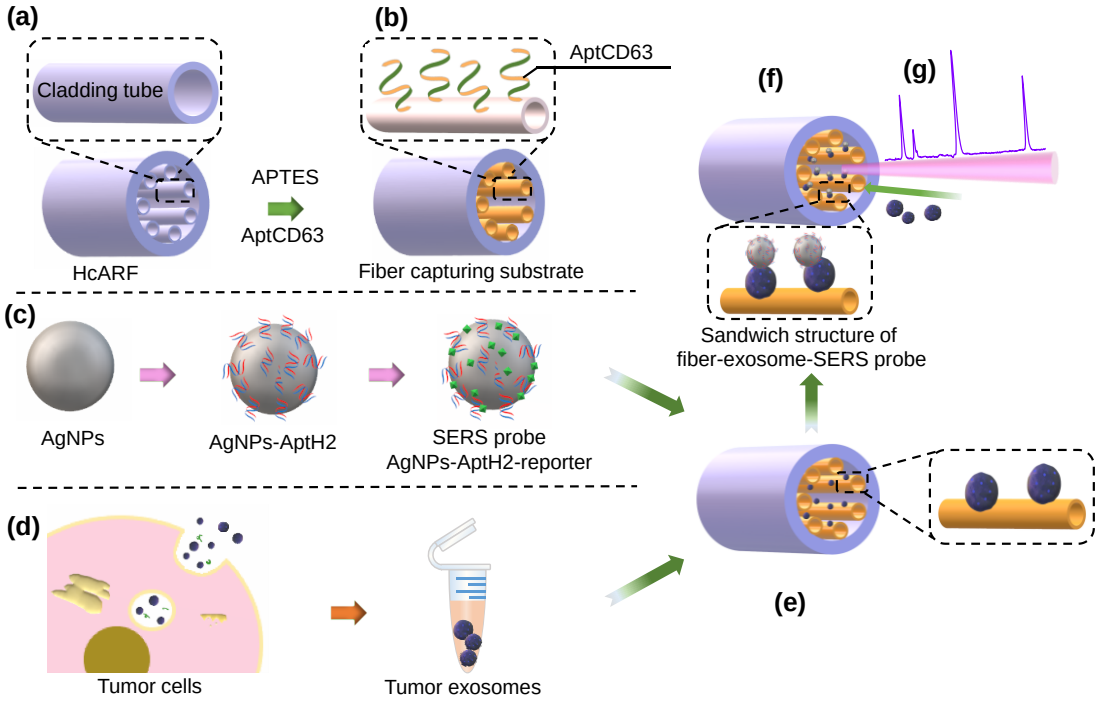

Fig. 3. Schematic diagram of the working principle of HcARF sensor. The inner wall of the fiber **(a)** is first aminated with APTES followed by functionalization with anti-CD63 aptamer **(b)**. After construction of cancer marker specific SERS probe **(c)**, and cancer cell derived exosomes are isolated **(d)**, exosome suspension is streamed in the fiber channel, and thus captured by the fiber **(e)**, subsequently, the SERS probe is introduced to the fiber channel. At this stage, the SERS probe can specifically recognize and bind to the cancer-related exosomes captured on the fiber **(f)**. When the sensor is excited with a 785nm laser, Raman spectrum that reflects the existence of cancer exosomes can be recorded by a Raman spectrometer **(g).**

Exosomes are a subclass of extracellular vesicles (EVs) with a diameter of 40-160 nm generated in a cellular "endocytosis-fusion-exclusion" manner, and play a crucial role in cell communication and tissue microenvironment regulation. Exosomes can trace back to the originating cells, reflecting disease progression and prognosis, providing a way to monitor pathological changes of cells or tissues. Therefore, exosome analysis holds great potential to diagnosis, prognosis, and therapy.

Having demonstrated the robust Raman enhancement of HcARF, we then constructed a sensor for exosome identification and quantification. The sensor was designed based on a sandwiched structure via integration of SERS and ARF enhanced

Raman scattering (AERS) as shown in Fig. 3.

The major advantage of sandwich senor is that high specificity and sensitivity can be achieved without pretreatment of the sample, which can be time-consuming and error-prone. To construct the sensor, the inner wall of HcARF fiber is chemically coupled with CD63 aptamer (AptCD63) to form a capture substrate (Fig. 3b); meanwhile, a SERS probe that can specifically recognize cancer exosomes is fabricated, as shown in Fig. 3c. Then, cancer related exosomes (Fig. 3d) are streamed in the fiber microchannel and thus are captured on the inner surface of the fiber. When SERS probes are passed through the fiber channel (Fig. 3e), they will bind to the cancer-specific exosomes to form a sandwich structure of "fiber capturing substrate-exosomes-SERS probes" as shown in Fig. 3f. By detecting the light intensity back-scattered of the fiber after excitation with a 785nm laser, Raman signal can be detected (Fig. 3g). This is the first study using ARF enhanced Raman scattering for label-free cancer exosome detection. The proposed sensor would enable (a) high sensitivity through joint effect of SERS and AERS. (b) high specificity and thus label-free Raman detection. (c) direct sample application without pretreatment. (d) nano liter level sample consumption.

To construct the sensor, a capture DNA was first immobilized on the fiber wall. Fiber capturing substrate was fabricated based on the recognition ability of CD63 aptamer (CD63 is a class of surface proteins present in all types of exosomes) [34], which enables capturing of all types of exosomes in the sample including normal cell exosomes and cancer cell exosomes. CD63 aptamer (AptCD63, table S1 for sequence) was chemically coupled to the cladding tube walls of HcARF, please see Fig. S2 for the chemistry. The quantity of capturing aptamer modified on tube walls could determine the quantity of trapped exosomes in the sample. We used a fluorescently labeled CD63 aptamer (AptCD63-Cy5, table S1) to optimize the capturing aptamer quantity via

measuring the fluorescence intensity in the fiber after chemical coupling (the optical setup for measuring fluorescence in fiber is shown in Fig. S3). The fluorescence intensity increased as the AptCD63-Cy5 concentration elevated, and reached maximum at concentration of 20μM (Fig. 4a and Fig. S4). Therefore, 20μM of AptCD63 was used to construct the sensor for all the following experiments.

Subsequently, a SERS probe was constructed using Ag nanoparticles (AgNPs). A single strand DNA aptamer against HER2 (H2) protein (AptH2, table S2 for sequence) and a Raman reporter molecule (4-MBN) were covalently bonded to AgNPs to form the SERS probe (Fig. 3c). HER2 is a cancer marker, highly over-expressed in SkBr3 breast cancer cells and exosomes. TEM images of AgNPs-AptH2 showed a thin layer on the surface of AgNPs (Fig. 4b, c), the final diameter of the SERS probe was about 88 nm. The zeta potentials of AgNPs and AgNPs-AptH2 (Fig. 4d) were -10.08667 and -33.16667 mV, further confirming successful linkage. The UV-Vis extinction spectrum of AgNPs-AptH2 showed a slight redshift compared with AgNPs (Fig. 4e). The optimized concentrations of AptH2, 4-MBN and AgNPs were 0.179 μM, 50 μM and 0.027 nM, respectively, corresponding to a ratio of 6.63×10^{3}: 1.85×10^{6}: 1, see figure 4f & S5 for details.

To ensure the SERS probe performance, we isolated breast cancer cell SkBr3 derived exosomes and investigated the binding between SERS probe and exosomes. The particle size distribution and morphology of the isolated exosomes are shown in Fig. 4g & h and Fig. S6. The exosomes showed a typical vesicle structure with average dimension of 120 nm (91% exosomes are in range of 110-170nm). The synthesized SERS probe was mixed with isolated SkBr3 exosomes followed by TEM analysis. The morphology of probe-exosome complex was shown in Fig. 4i. Clearly, the SERS probe bound to SkBr3 exosome efficiently, in most cases, at 1:1 ratio.

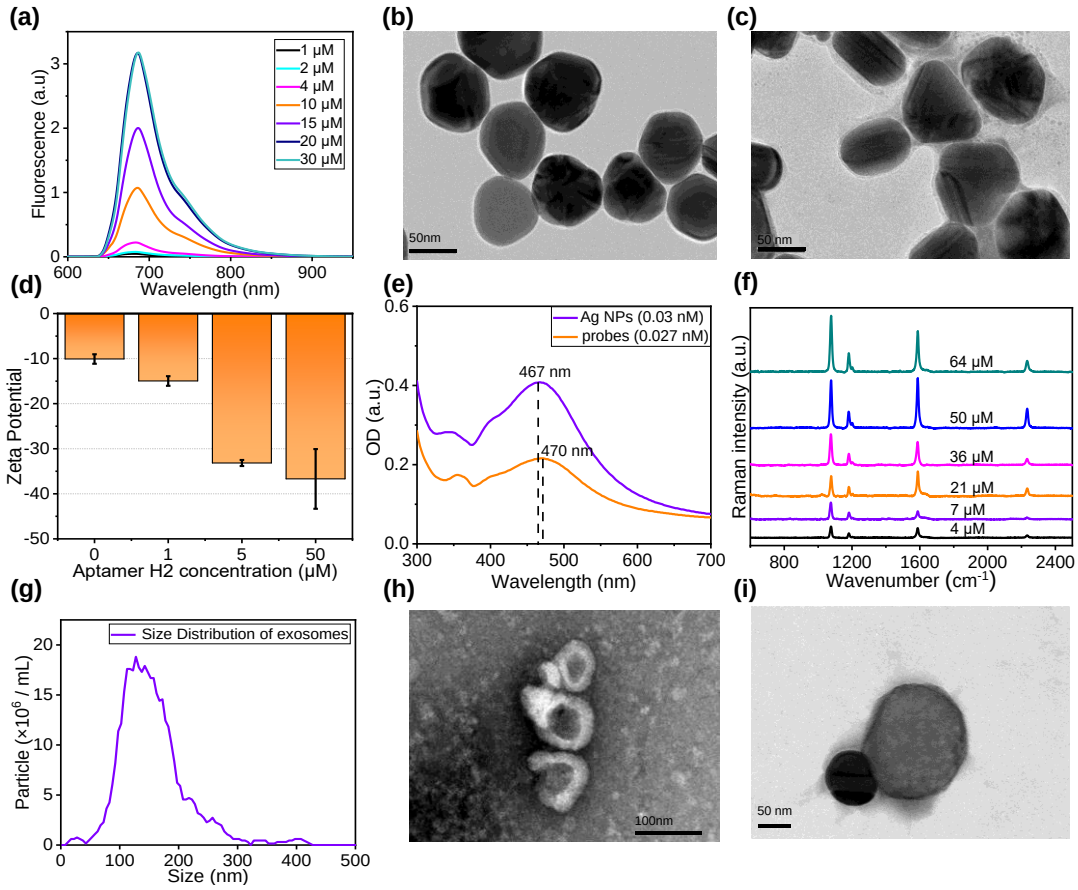

Fig. 4. Construction of the sensor. **(a)**. Dose-dependent fluorescence of Cy5-Apt$_{CD63}$ modified HcARF. **(b)** & **(c)**. Morphology of AgNPs prior (left) and post (right) AptH2 association. The scale bar is 50nm. **(d)** Zeta potentials of AptH2 modified AgNPs. **(e)**. UV-Vis absorption of AgNPs (0.03nM) and SERS probe (0.027nM). **(f)**. Raman spectra of SERS probe with various concentrations of 4-MBN molecule. **(g)**. Size distribution of isolated cancer exosomes. **(h)** Morphology of the isolated cancer exosomes viewed by TEM. **(i)**. A heterodimer of a SERS probe and an exosome.

Cancer exosome sensing

As proof-of-concept, we conducted exosome sensing using the platform. The exosome suspension was reconstituted into various concentrations, and subsequently streamed in a 10cm ARF sensor followed by introduction of SERS probe. After the redundant probes were washed out, the fiber sensor was excited with a 785nm laser. The Raman signal intensified as the exosome concentration increased as shown in Fig. 5a. The intensities (after subtraction of the background) of Raman mode at wavenumbers of 1075 cm^{-1} and 1585 cm^{-1} were plotted as a function of exosome

concentration (Fig. 5b). Clearly, the Raman signals of the two modes increased as the exosome numbers increased in a dose-dependent manner. The peak at wavenumber of 1075cm^{-1} was used to evaluate the quantity of exosomes. In the exosomes concentration range of 8-1600 particles/μL, the Raman signal showed a good linearity with the exosome concentration, Fig. 5b inset. The simulated limit of detection (LoD) was 2.2 particles/μL (LoD=3δ/S), which means single exosome detection can be achieved since only about 253nL sample is required for a 10cm HcARF fiber. Fig. 5c displays the high-resolution SEM images of the fiber wall prior (i) and post exosome capture (ii) and post SERS probe binding (iii).

To validate the results, we performed a number of control experiments, as shown in Fig. 5d. No Raman signal was detected in the absence of CD63 aptamer (dark red line) or exosomes (dark cyan line), which ruled out the possibility of false positive results. When the AptH2 aptamer on the SERS probes was replaced with a random DNA sequence (dark yellow line, table S1 for sequence), no detectable Raman signal was obtained either, indicating the high specificity of the system toward cancer marker HER2 overexpressed exosomes. The sensor was fairly robust. Electric field (15 V/m) and magnetic field (10 μT) could not interfere with the Raman signal (Fig. S7), suggesting a benefit of optical fiber sensing (electric and magnetic field would be supposed to interfere with some assays, for instance, electrochemical sensors).

The selectivity of the sensor was investigated using a panel of cancer cell (breast cancer cell lines of SkBr3, MDA-MB-231, T47D and pancreatic cancer cell line Panc-1) derived exosomes. A non-cancerous cell line NIH3T3 derived exosomes were also tested for comparison. As shown in Fig. 5d, the Raman intensity of SkBr3 exosomes was significantly stronger than that of other cancer cell derived exosomes, while no detectable Raman signal was obtained for NIH3T3 derived exosomes. The differences

are statistically significant, Fig. 5e. Therefore, the proposed sensor could selectively distinguish exosomes secreted by H2 overexpressing cancer cells, holding great potential for clinical diagnosis.

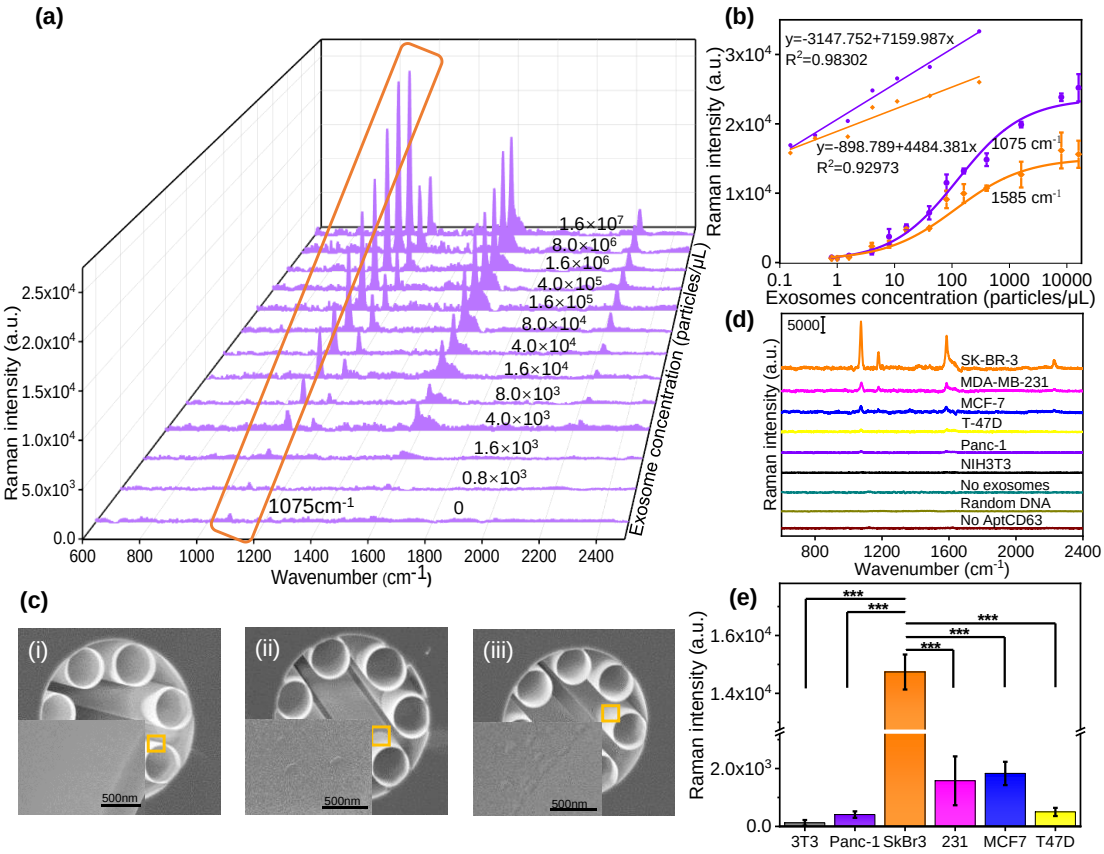

Fig. 5. Cancer exosome sensing using the HcARF-based platform. **(a)**. Raman spectra at various concentrations of exosome suspension. **(b)**. Dose-dependent response of Raman signal at 1075 cm^{-1} and 1585 cm^{-1}. **(c)**. SEM images of the fiber wall before exosome capture (i), after exosome capture (ii), and after SERS probe binding (iii). **(d)**. Specificity and selectivity of the fiber sensor. **(e)**. Statistical analysis of the data of (d) (n=3). *** indicates $p<0.001$.

Exosome surface protein profiling

Exosomes are highly heterogeneous in molecular composition [35-38], and their surface proteins bear characteristics of their tissues of origin [39, 40], rendering specific subclasses of these vesicles promising to demonstrate pathology affecting specific tissues [41-43]. The distinct characteristics of exosomal surface markers in different diseases also manifest them a promising basis for disease classification. Therefore, we

investigated the surface protein profiling of various types of exosomes derived from cancer cells.

To this end, we fabricated a panel of SERS probes, as shown in table S2. Each probe was designed to recognize a specific surface marker of cancer cell (ER, MUC1, EGFR and EpCAM) and attached with a distinct Raman molecule (4-Mpy, 2NAT, 4-NBT and MGITC, respectively). We measured the protein expression on the surface of six types of cellular exosomes, including NIH3T3, Panc 01, MDA-MB-231, MCF7 and T47D.

Different types of exosomes isolated from different cell culturing media were reconstituted to the same concentration of 400 particles/μl, and streamed in the fiber channel, followed by introduction of SERS probe and acquisition of the Raman signal. The obtained data were shown in Fig. 6. With ER-specific SERS probe, the fiber sensor gave rise to the highest response to exosomes of MCF7 (1004 cm^{-1} wavenumber), Fig. 6a. Other exosomes only generated low level Raman signal, the difference is statistically significant, Fig. S8a. With MUC1-specific SERS probe, Fig. 6b and Fig. S8b, highest response was observed for exosomes of MCF7 and MDA-MB-231 cells (1378cm^{-1} wavenumber), while exosomes of T47D resulted in moderate Raman response and exosomes of other three cell lines resulted in the lowest Raman signal. With EGFR-specific SERS probe, the highest response was observed for exosome of MDA-MB-231 cell (wavenumber 1332 cm^{-1}), Fig. 6c and Fig. S8c, while moderate responses were observed for exosomes of SkBr3 and Panc-1, and lowest responses were observed for other three type of exosomes. With EpCAM-specific SERS probe, the highest response was obtained from exosome of SkBr3 cell (wavenumber 1616 cm^{-1}), other exosomes hardly generated any Raman response, Fig. 6d and Fig. S8d.

The data were plotted in a heatmap as shown in Fig. 6e(i). Analysis of the protein expression profile of different types of exosomes reveals that the five cancer markers

exist in all five cancer cell line derived exosomes, expression levels are distinctly different though. These data verify the capability of fiber sensor to differentiate the subtle variation of protein levels in exosomes from different cell types. The data indicate that the panel of exosomal protein information can be used to identify the source cells of exosomes, please refer to Fig. 6e(ii)). For example, because EpCAM and HER2 were shown to be cancer biomarkers, their exosomal levels can serve as the first criterion to distinguish HER2(+) cancer cells from normal and other cancerous cells (Fig. 6e); similarly, ER and MUC1 can be used to distinguish MCF7 type of cancer from others. Consequently, the SERS-based ARF sensor detection of a panel of biomarkers is able to distinguish exosomes secreted from five different cells.

Finally, the feasibility of multiplexed detection of different types of exosomes were also investigated by taking advantages of the platform. The mixture of three types of exosomes (SkBr3, MCF7 and MDA-MB-231) at 1:1:1 ratio was filled in the fiber channel after AptCD63 was fixed on the fiber wall. Then a mixture of three SERS probes for HER2, ER and MUC1 was streamed in the channel. Subsequently, the Raman signal was acquired with excitation of a 785nm laser, as shown in Fig. 6f. The intensities of the dominant bands highlighted in Fig. 6f, i.e. 1004cm^{-1} for ER, 1378cm^{-1} for MUC1, and 2223cm^{-1} for HER2 (please note, 1075 cm^{-1} was used for specific analysis of HER2-positive exosome in the aforementioned single probe assay. For multiplexed assay, since MUC1 probe shows a Raman mode at 1068cm^{-1}, very close to 1075cm^{-1}, to avoid ambiguity, 2223cm^{-1} mode was chosen to distinguish HER2 from others) can simultaneously reflect the presence of the corresponding exosomes of MCF7, MDA-MB-231 and SkBr3. The success of the simultaneous multiple detection of exosomes is significant for the application of this method in clinical diagnostics.

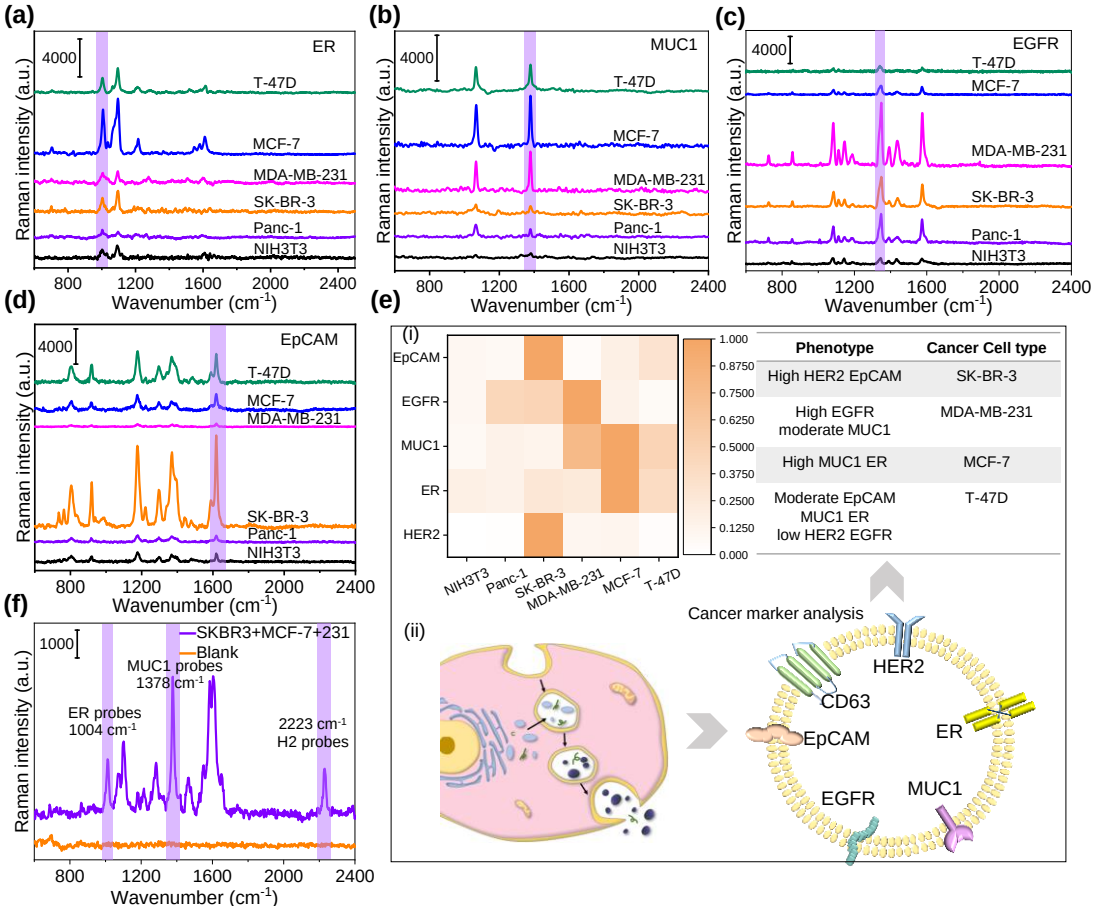

Fig. 6. Cancer exosome differentiation via surface marker profiling. **(a), (b), (c) & (d)**. Raman spectra in response to different types of exosomes using SERS probes specific to cancer markers of ER, MUC1, EGFR and EpCAM, respectively. **(e)**. (i) Heat map indicating the expression levels of five different cancer markers (EpCAM, EGFR, MUC1, ER, HER2) of exosomes from six different cell lines (four breast cancer cell lines: SkBr3, MCF7, T47D, MDA-MB-231, one pancreatic cancer line Panc-1, and one non-cancerous cell line NIH-3T3). Cancer marker levels are indicated by the Raman signal intensities at specific wavenumber per unit concentration of exosomes. Right panel is a summary of the phenotype. (ii). Illustration of the origin of exosomes possessing different biomarkers. **(f)**. Multiplexed detection of different types of exosomes.

Conclusions

In summary, we have investigated the Raman enhancing effect of hollow-core anti-resonant optical fiber (HcARF), several-orders-of-magnitude enhancement was achieved owing to the specific light-confinement property and cumulative effect of the ARF fiber. Stemmed from here, a sandwich structured fiber sensor was developed. Sensitive detection of breast cancer SkBr3 secreted exosomes down to single exosome

level was realized. Analyzing the Raman signals in response to a panel of cancer exosomes allow us to distinguish different types of cancer. It is well known that exosomes carry proteins and nucleic acids related to the types and corresponding metabolic status of the parent cells. Such exosomal information can be considered as a fingerprint of its parent cells and be potentially used for the identification of cancer cells. The proposed platform provides a way to further enhance Raman signal on the top of SERS, holding great potential for Point-of-care testing (POCT).

SERS-ARF platform could also be used for therapeutic purposes for the delivery to specific parts of the body accurately and quickly and monitoring drug treatment response in real-time. The superiority SERS tags over the fluorescent counterparts in terms of multiplexing capability, low toxicity and clearance efficiency is well documented in *in vivo* studies, the combination of SERS tag with state-of-the-art HcARF would open up a new door for super sensitive biomarker detection. Hereafter, such platform could be exploited in the future to realize a clinically viable, real time sensing tool.

Since the discovery of SERS, large efforts have been devoted to the improvement of enhancement factor (EF). Our findings provide an efficient way to additionally enhance the Raman signal on the top of SERS. Taken together, the ongoing tremendous development in HcARF combined with smart design of SERS tags could ultimately lead to a rapid, sensitive diagnostic tool for the patients.

ASSOCIATED CONTENT

Supporting Information Available

The following files are available free of charge.

Setup for Raman signal acquisition from an ARF fiber (Figure S1); chemical method to deposit CD63 aptamer on the fiber wall (Figure S2); the setup for fluorescence measurement of AptCD63-Cy5 (Figure S3); dose-dependent fluorescence intensities of AptCD63-Cy5 (Figure S4); optimization of the Raman molecule concentration (Figure S5); high-resolution TEM images of SkBr3 exosomes (Figure S6); effects of electric and magnetic fields on Raman intensity (Figure S7); the expression of ER, MUC1, EGFR, EpCAM in six cell lines (Figure S8); supplementary tables, supplementary methods

AUTHOR INFORMATION

Corresponding Author

Xiu-Hong Wang, Prof. Laboratory for Biomedical Photonics, Institute of Laser Engineering, Faculty of Materials and Manufacturing, Key Laboratory of Trans-scale Laser Manufacturing Technology, Ministry of Education, Beijing Engineering Research Center of Laser Technology, Beijing University of Technology, Beijing 100124 China

Email: wxh2012@bjut.edu.cn

Authors

Zhiwen Xia - Laboratory for Biomedical Photonics, Institute of Laser Engineering, Faculty of Materials and Manufacturing, Beijing University of Technology; Beijing 100124 China

Xin Zhang - Laboratory for Advanced Laser Technology and Applications, Institute of Laser Engineering, Faculty of Materials and Manufacturing, Beijing University of Technology; Beijing 100124 China

Jingyuan Yao - Laboratory for Advanced Laser Technology and Applications, Institute of Laser Engineering, Faculty of Materials and Manufacturing, Beijing University of Technology; Beijing 100124 China

Zihao Liu - Laboratory for Biomedical Photonics, Institute of Laser Engineering, Faculty of Materials and Manufacturing, Beijing University of Technology; Beijing 100124 China

Yulong Jin - Laboratory for Advanced Laser Technology and Applications, Institute of Laser Engineering, Faculty of Materials and Manufacturing, Beijing University of Technology; Beijing 100124 China

Huabing Yin - Department of Biomedical Engineering, James Watt School of Engineering, University of Glasgow, Glasgow G12 8LT, the United Kingdom

Pu Wang - Laboratory for Advanced Laser Technology and Applications, Institute of Laser Engineering, Faculty of Materials and Manufacturing, Beijing University of Technology; Beijing 100124 China

Author Contributions

XH Wang proposed the project and designed the experiments. Z Xia, X Zhang, J Yao and Y Jin conducted the construction and measurements. Z. Xia wrote the manuscript. XH Wang performed modifications of the manuscript. All authors participated in the data analysis and discussions. XH Wang and P Wang supervised the project.

Notes

The authors declare no competing financial interest.

ACKNOWLEDGMENTS

This research was supported in part by the National Natural Science Foundation of

China (No: 92053116 & No: 62035002), the National Research and Development Program of China (No. 2017YFB0405200), and Beijing Natural Science Foundations (L182011, 4192013). The authors thank BJUT Core Facilities for technical support.

References:

(1) Chen, X.; Ding, W.; Wang, Y.; Gao, S.; Xu, F.; Xu, H.; Hong, Y.; Sun, Y.; Wang, P.; Lu, Y.et al. High-fidelity, low-latency polarization quantum state transmissions over a hollow-core conjoined-tube fiber at around 800 nm. *Photonics research (Washington, DC)* **2021**, 9, 460.

(2) Hong, Y. F.; Gao, S. F.; Ding, W.; Zhang, X.; Jia, A. Q.; Sheng, Y. L.; Wang, P.; Wang, Y. Y. Highly Birefringent Anti‐Resonant Hollow‐Core Fiber with a Bi‐Thickness Fourfold Semi‐Tube Structure. *Laser Photonics Rev.* **2022**, 16, 2100365.

(3) Taranta, A.; Numkam Fokoua, E.; Abokhamis Mousavi, S.; Hayes, J. R.; Bradley, T. D.; Jasion, G. T.; Poletti, F. Exceptional polarization purity in antiresonant hollow-core optical fibres. *Nat. Photonics* **2020**, 14, 504-510.

(4) Ni, W.; Yang, C.; Luo, Y.; Xia, R.; Lu, P.; Hu, D. J. J.; Danto, S.; Shum, P. P.; Wei, L. Recent Advancement of Anti-Resonant Hollow-Core Fibers for Sensing Applications. *Photonics* **2021**, 8, 128.

(5) De Acha, N.; Socorro-Leránoz, A. B.; Elosúa, C.; Matías, I. R. Trends in the Design of Intensity-Based Optical Fiber Biosensors (2010–2020). *Biosensors* **2021**, 11, 197.

(6) Qiao, P.; Wang, XH.; Gao, S.; Yin, X.; Wang, Y.; Wang, P. Integration of black phosphorus and hollow-core anti-resonant fiber enables two-order magnitude enhancement of sensitivity for bisphenol A detection. *Biosensors and Bioelectronics* **2020**, *149*, 111821.

(7) Zhao, P.; Ho, H. L.; Jin, W.; Fan, S.; Gao, S.; Wang, Y. Hollow-core fiber photothermal methane sensor with temperature compensation. *Opt. Lett.* **2021**, 46, 2762-2765.

(8) Zhao, P.; Zhao, Y.; Bao, H.; Ho, H. L.; Jin, W.; Fan, S.; Gao, S.; Wang, Y.; Wang, P. Mode-phase-difference photothermal spectroscopy for gas detection with an anti-resonant hollow-core optical fiber. *Nat. Commun.* **2020**, 11.

(9) Zhao, Y.; Qi, Y.; Lut, H.; Gao, S.; Wang, Y.; Jin, W. Photoacoustic Brillouin spectroscopy of gas-filled anti-resonant hollow-core optical fibers. *Optica* **2021**, 8, 532-538.

(10) Guo, X.; Zhang, X.; Liu, Z.; Dong, Z.; Xia, Z.; Meng, X.; Wang, P.; Wang, X. Strong light-matter interaction in hollow-core microfiber for multiplex sensing of environmental hazards. *Sensors and Actuators B: Chemical* **2022**, 371, 132613.

(11) Demirel, G.; Usta, H.; Yilmaz, M.; Celik, M.; Alidagi, H. A.; Buyukserin, F. Surface-enhanced Raman spectroscopy (SERS): an adventure from plasmonic metals to organic semiconductors as SERS platforms. *Journal of materials chemistry. C, Materials for optical and electronic devices* **2018**, 6, 5314-5335.

(12) Lee, D. Y.; Park, C.; Choi, J.; Koo, Y.; Kang, M.; Jeong, M. S.; Raschke, M. B.; Park, K. Adaptive tip-enhanced nano-spectroscopy. *Nat. Commun.* **2021**, 12.

(13) Hümmer, T.; Noe, J.; Hofmann, M. S.; Hänsch, T. W.; Högele, A.; Hunger, D. Cavity-enhanced Raman microscopy of individual carbon nanotubes. *Nat. Commun.* **2016**, 7.

(14) Han, Y.; Tan, S.; Oo, M. K. K.; Pristinski, D.; Sukhishvili, S.; Du, H. Towards Full-Length Accumulative Surface-Enhanced Raman Scattering-Active Photonic Crystal Fibers. *Adv. Mater.* **2010**, 22, 2647-2651.

(15) Hanf, S.; Bögözi, T.; Keiner, R.; Frosch, T.; Popp, J. Fast and Highly Sensitive Fiber-Enhanced Raman Spectroscopic Monitoring of Molecular H2 and CH4 for Point-of-Care Diagnosis of Malabsorption Disorders in Exhaled Human Breath. *Anal. Chem.* **2015**, 87, 982-988.

(16) Hanf, S.; Keiner, R.; Yan, D.; Popp, J.; Frosch, T. Fiber-Enhanced Raman Multigas Spectroscopy: A Versatile Tool for Environmental Gas Sensing and Breath Analysis. *Anal. Chem.* **2014**, 86, 5278-5285.

(17) U. S., D.; Fu, C. Y.; Soh, K. S.; Ramaswamy, B.; Kumar, A.; Olivo, M. Highly sensitive SERS detection of cancer proteins in low sample volume using hollow core photonic crystal fiber. *Biosensors and Bioelectronics* **2012**, 33, 293-298.

(18) Yan, D.; Frosch, T.; Kobelke, J.; Bierlich, J.; Popp, J.; Pletz, M. W.; Frosch, T. Fiber-Enhanced Raman Sensing of Cefuroxime in Human Urine. *Anal. Chem.* **2018**, 90, 13243-13248.

(19) Khetani, A.; Momenpour, A.; Alarcon, E. I.; Anis, H. Hollow core photonic crystal fiber for monitoring leukemia cells using surface enhanced Raman scattering (SERS. *Biomed. Opt. Express* **2015**, 6, 4599-4609.

(20) Dinish, U. S.; Beffara, F.; Humbert, G.; Auguste, J. L.; Olivo, M. Surface‐enhanced Raman scattering‐active photonic crystal fiber probe: Towards next generation liquid biopsy sensor with ultra high sensitivity. *J. Biophotonics* **2019**, 12.

(21) Humbert, G.; Knight, J.; Bouwmans, G.; Russell, P.; Williams, D.; Roberts, P.; Mangan, B. Hollow core photonic crystal fibers for beam delivery. *Opt. Express* **2004**, 12, 1477-1484.

(22) Gao, D.; Yang, X.; Teng, P.; Luo, M.; Zhang, H.; Liu, Z.; Yang, J.; Li, Z.; Wen, X.; Yuan, L.et al. In-fiber optofluidic online SERS detection of trace uremia toxin. *Opt. Lett.* **2021**, 46, 1101-1104.

(23) Chu, Q.; Jin, Z.; Yu, X.; Li, C.; Zhang, W.; Ji, W.; Lin, B.; Shum, P. P.; Zhang, X.; Wang, G. Volumetric enhancement of Raman scattering for fast detection based on a silver-lined hollow-core fiber. *Opt. Express* **2019**, 27, 10370.

(24) Gao, D.; Yang, X.; Teng, P.; Kong, D.; Liu, Z.; Yang, J.; Luo, M.; Li, Z.; Wen, X.; Yuan, L.et al. On-line SERS detection of adenine in DNA based on the optofluidic in-fiber integrated GO/PDDA/Ag NPs. *Sensors and Actuators B: Chemical* **2021**, 332, 129517.

(25) Gao, D.; Yang, X.; Teng, P.; Kong, D.; Liu, Z.; Yang, J.; Luo, M.; Li, Z.; Wen, X.; Yuan, L.et al. On-line SERS detection of adenine in DNA based on the optofluidic in-fiber integrated GO/PDDA/Ag NPs. *Sensors and Actuators B: Chemical* **2021**, 332, 129517.

(26) Liu, X. L.; Ding, W.; Wang, Y. Y.; Gao, S. F.; Cao, L.; Feng, X.; Wang, P. Characterization of a liquid-filled nodeless anti-resonant fiber for biochemical sensing. *Opt. Lett.* **2017**, 42, 863-866.

(27) Cubillas, A. M.; Jiang, X.; Euser, T. G.; Taccardi, N.; Etzold, B. J. M.; Wasserscheid, P.; Russell, P. S. J. Photochemistry in a soft-glass single-ring hollow-core photonic crystal fibre. *Analyst* **2017**, 142, 925-929.

(28) Ding, W.; Wang, Y. Semi-analytical model for hollow-core anti-resonant fibers. *Frontiers in Physics* **2015**, 3.

(29) Liu, X. L.; Ding, W.; Wang, Y. Y.; Gao, S. F.; Cao, L.; Feng, X.; Wang, P. Characterization of a

liquid-filled nodeless anti-resonant fiber for biochemical sensing. *Opt. Lett.* **2017**, 42, 863-866.

(30) Chen, K.; Zhou, X.; Cheng, X.; Qiao, R.; Cheng, Y.; Liu, C.; Xie, Y.; Yu, W.; Yao, F.; Sun, Z.et al. Graphene photonic crystal fibre with strong and tunable light–matter interaction. *Nat. Photonics* **2019**, 13, 754-759.

(31) Sun, Y.; Zhang, N.; Han, C.; Chen, Z.; Zhai, X.; Li, Z.; Zheng, K.; Zhu, J.; Wang, X.; Zou, X.et al. Competitive immunosensor for sensitive and optical anti-interference detection of imidacloprid by surface-enhanced Raman scattering. *Food Chem.* **2021**, 358, 129898.

(32) Pearman, W. F.; Carter, J. C.; Angel, S. M.; Chan, J. W. Multipass Capillary Cell for Enhanced Raman Measurements of Gases. *Appl. Spectrosc.* **2008**, 62, 285-289.

(33) Chu, Q.; Jin, Z.; Yu, X.; Li, C.; Zhang, W.; Ji, W.; Lin, B.; Shum, P. P.; Zhang, X.; Wang, G. Volumetric enhancement of Raman scattering for fast detection based on a silver-lined hollow-core fiber. *Opt. Express* **2019**, 27, 10370.

(34) Mathieu, M.; Névo, N.; Jouve, M.; Valenzuela, J. I.; Maurin, M.; Verweij, F. J.; Palmulli, R.; Lankar, D.; Dingli, F.; Loew, D.et al. Specificities of exosome versus small ectosome secretion revealed by live intracellular tracking of CD63 and CD9. *Nat. Commun.* **2021**, 12.

(35) Tauro, B. J.; Greening, D. W.; Mathias, R. A.; Mathivanan, S.; Ji, H.; Simpson, R. J. Two Distinct Populations of Exosomes Are Released from LIM1863 Colon Carcinoma Cell-derived Organoids. *Mol. Cell. Proteomics* **2013**, 12, 587-598.

(36) Poliakov, A.; Spilman, M.; Dokland, T.; Amling, C. L.; Mobley, J. A. Structural heterogeneity and protein composition of exosome-like vesicles (prostasomes) in human semen. *The Prostate* **2009**, 69, 159-167.

(37) Yuana, Y.; Koning, R. I.; Kuil, M. E.; Rensen, P. C. N.; Koster, A. J.; Bertina, R. M.; Osanto, S. Cryo-electron microscopy of extracellular vesicles in fresh plasma. *Journal of extracellular vesicles* **2013**, 2, 21494.

(38) Willms, E.; Johansson, H. J.; Mäger, I.; Lee, Y.; Blomberg, K. E. M.; Sadik, M.; Alaarg, A.; Smith, C. I. E.; Lehtiö, J.; EL Andaloussi, S.et al. Cells release subpopulations of exosomes with distinct molecular and biological properties. *Sci. Rep.-UK* **2016**, 6.

(39) Larssen, P.; Wik, L.; Czarnewski, P.; Eldh, M.; Löf, L.; Ronquist, K. G.; Dubois, L.; Freyhult, E.; Gallant, C. J.; Oelrich, J.et al. Tracing Cellular Origin of Human Exosomes Using Multiplex Proximity Extension Assays. *Mol. Cell. Proteomics* **2017**, 16, 1547.

(40) Castillo, J.; Bernard, V.; San Lucas, F. A.; Allenson, K.; Capello, M.; Kim, D. U.; Gascoyne, P.; Mulu, F. C.; Stephens, B. M.; Huang, J.et al. Surfaceome profiling enables isolation of cancer-specific exosomal cargo in liquid biopsies from pancreatic cancer patients. *Ann. Oncol.* **2018**, 29, 223-229.

(41) Herreros-Villanueva, M.; Bujanda, L. Glypican-1 in exosomes as biomarker for early detection of pancreatic cancer. *Annals of translational medicine* **2016**, 4, 64.

(42) Tavoosidana, G.; Ronquist, G.; Darmanis, S.; Yan, J.; Carlsson, L.; Wu, D.; Conze, T.; Ek, P.; Semjonow, A.; Eltze, E.et al. Multiple recognition assay reveals prostasomes as promising plasma biomarkers for prostate cancer. *Proceedings of the National Academy of Sciences* **2011**, 108, 8809-8814.

(43) Peinado, H.; Alečković, M.; Lavotshkin, S.; Matei, I.; Costa-Silva, B.; Moreno-Bueno, G.; Hergueta-Redondo, M.; Williams, C.; García-Santos, G.; Ghajar, C. M.et al. Melanoma exosomes educate bone marrow progenitor cells toward a pro-metastatic phenotype through MET. *Nat. Med.* **2012**, 18, 883-891.

TOC graphic（For TOC only）：